Available online at www.sciencedirect.com
ScienceDirect
International Journal of Heat and Fluid Flow 29 (2008) 830–840
International Journal of HEAT AND FLUID FLOW
www.elsevier.com/locate/ijhff

Dynamic wall-shear stress measurements in turbulent pipe flow using the micro-pillar sensor MPS^3

Sebastian Große *, Wolfgang Schröder

Institute of Aerodynamics, RWTH Aachen University, Wüllnerstraße 5-7, D-52062 Aachen, Germany

Received 15 October 2007; received in revised form 17 January 2008; accepted 24 January 2008
Available online 6 March 2008

Abstract

The micro-pillar wall-shear stress sensor MPS^3 has been used to measure the dynamic wall-shear stress in turbulent pipe flow. The sensor device consists of a flexible micro-pillar which extends from the wall into the viscous sublayer. The pillar-tip deflection caused by the exerting fluid forces serves as a measure for the local wall-shear stress. The pillar is statically calibrated in linear shear flow. A second-order estimate of the pillar dynamic response based on experimentally determined sensor characteristics shows the potential of the present sensor configuration to also measure the dynamic wall-shear stress. The quality of the micro-pillar shear stress sensor MPS^3 to correctly determine the skin friction will be shown by measuring the wall friction in a well-defined fully developed turbulent pipe flow at Reynolds numbers Re_b based on the bulk velocity U_b and the pipe diameter D in the range of $Re_b = 10,000$–$20,000$. The results demonstrate a convincing agreement of the mean and dynamic wall-shear stress obtained with the MPS^3 sensor technique with analytical, experimental, and numerical results from the literature.

Keywords: Wall-shear stress measurement; Skin friction measurement; Micro-pillar shear stress sensor MPS^3; Turbulent pipe flow

1. Introduction

The assessment of the wall-shear stress $\tau = \eta \cdot \partial u/\partial y|_{wall}$ has been the subject of many experimental and numerical studies in the last decades. Herein, η is the dynamic fluid viscosity, u the streamwise velocity, and y the distance from the wall. The knowledge of the mean wall-shear stress is a necessary prerequisite to determine the friction velocity $u_\tau = (\tau/\rho)^{1/2}$ as one of the fundamental turbulence scaling parameters. Herein, ρ is the fluid density. The temporal and spatial shear stress distribution is related to turbulent flow structures in the vicinity of the wall and is as such of major importance for the basic understanding of the development of near-wall turbulent events.

During the last decades many different wall-shear stress sensors have been developed, which can be divided into two major categories based on the measurement principle, the so-called direct and indirect techniques. Wall-implemented floating elements and oil-film techniques are the most common representatives of the former technique. Indirect techniques require an empirical or theoretical relation between the wall-shear stress and the quantity measured by the sensor. Typically this relation is only valid for very specific conditions. The most common dependences used are on the one hand, the Reynolds analogy, describing the correlation between the wall-normal heat transfer and the momentum transfer and on the other hand, the relation between the near-wall velocity gradient of turbulent flows in the vicinity of the surface and the wall-shear stress.

To discuss the whole diversity of shear stress sensors developed in the last decades is beyond the scope of this paper and the reader is referred to the comprehensive reviews on the development of wall-shear stress devices given by Fernholz et al. (1996), Löfdahl and Gad-el-Hak (1999) and Naughton and Sheplak (2002). Here, we would like to focus mainly on the description of sensor designs,

* Corresponding author.
E-mail address: s.grosse@aia.rwth-aachen.de (S. Große).

0142-727X/$ - see front matter © 2008 Elsevier Inc. All rights reserved.
doi:10.1016/j.ijheatfluidflow.2008.01.008

which are based on the same measurement principle as the micro-pillar wall-shear stress sensor used in the present study.

In recent years bionics and especially the fish lateral line flow sensor and filiform hair sensors have inspired researchers to develop artificial hair cell sensors based on flexible cantilevers and micro-posts. A very comprehensive review on the mechanics of these sensor structures is given by Humphrey and Barth (2007).

Fan et al. (2002) and Chen et al. (2003) report different kinds of flow cantilevers and micro-posts. One type of these cantilevers consists of L-shaped structures, the vertical part of which exceeds into the flow field. The bending of the cantilever due to the flow forces is detected by strain gages in the base of the horizontal cantilever arm. Since single cantilevers can only detect unidirectional velocities the authors grouped arrays of sensors with different frontal orientation. More recently, Tucker et al. (2006) reported a sensor structure based on a cylindrical micro-post made of SU-8 epoxy. The post deflection is measured by silicon piezoresistive strain gages in the sensor base. Again the sensor allows to determine only one flow direction. To detect the two-dimensional flow field distribution, the authors use neighboring pairs of sensors with orthogonally oriented strain gages. Engel et al. (2006) have presented a polyurethane artificial hair cell sensor. The authors use structures similar to the micro-pillar sensor and position the posts on commercial conductive polyurethane force sensitive resistors (FSR) to detect the bending of the post structure. The cylindrical version of their posts showed a remaining on to off-axis sensitivity ratio of 14.2 dB but sensor structures with improved geometries showed the desirable off-axis mechanical insensitivity.

A hair-like sensor is reported by Dijkstra et al. (2005) and Krijnen et al. (2006). These authors use SU-8 cricket-sensory hairs to detect drag forces on the sensor structure. This technique is not used to detect the wall-shear stress but to measure acoustic pressure disturbances. The deflection is detected capacitively at the sensor-hair base. Using sensor heights of up to 1 mm the authors deliberately protrude the local boundary layer to achieve a high enough sensitivity of the sensor structure.

Although the sensor presented by Kimura et al. (1999) and Lin et al. (2004) is a thermal sensor, it should be briefly described here, since these authors have established a sensor design that allows to visualize and measure the two-dimensional wall-shear stress distribution. The authors succeeded in positioning 25 sensors in the spanwise direction achieving a spatial resolution of 300 μm. Three such sensor lines have been installed in the streamwise direction. The spatial resolution along this direction was impeded by the necessary positioning of the hot-wire connections. The results presented by the authors show the coexistence of regions of lower and higher wall-shear stresses. These distributions represent the 'foot-prints' of very near-wall turbulent coherent structures such as low-speed and high-speed streaks that are aligned in the viscous sublayer of turbulent boundary layers and represent one of the first evolutionary stages in the auto-generative cycle of turbulence production in turbulent flows.

Note, similar findings could be detected by an array of micro-pillar shear stress sensors in a recent study (Große and Schröder, submitted for publication). The sensor consists of 17×25 pillars in the streamwise and spanwise direction, respectively. The lateral spacing of 250 μm corresponds to approximately 5.2 viscous units at the Reynolds number in the experiment. It could be evidenced that the low-shear regions have the shape of narrow meandering bands, interrupted by local high-shear regions laying in between these structures. While the spanwise width of the structures can well be captured with the sensor, the dimension in the streamwise direction exceeds the field of view of the sensor geometry. However, applying Taylor's hypothesis allows to roughly estimate the streamwise extension to be of the order of 1000 l^+.

It can be stated that most existing sensors are one-directional devices that require the necessity of secondary electronic structures to be implemented in the wall, thereby impeding the spatial resolution and limiting the arrays to a maximum number of sensors due to constructional constraints. Therefore, it can be stated that the determination of the planar wall-shear stress distribution is still an open issue in the field of experimental fluid mechanics.

The possibility of a highly resolving spatial detection of the two-dimensional wall-shear stress distribution is the great potential of the micro-pillar shear stress sensor MPS^3 described in this paper.

First experiments in laminar shear flow and a first introduction to the sensor concept are given in Brücker et al. (2005), demonstrating the general feasibility of the sensor concept as a shear flow sensor. The use of micro-pillars as force sensors for drag forces acting on micro-particles in shear flows has been demonstrated in Große et al. (2006). A detailed description of the pillar mechanics, a discussion of the achievable sensitivity and accuracy as well as a first application of the sensor to determine the mean wall-shear stress in turbulent pipe flow is given in Große and Schröder (2008).

It is the main objective of this paper to apply the wall-shear stress sensor to turbulent shear flows and to assess the quality of the MPS^3 sensor by quantitatively capturing the dynamic wall-shear stress in turbulent pipe flow. In Section 2, the sensor concept will be discussed. Subsequently, the flow facility and details of the micro-pillar sensor setup are briefly described. Then, the results of the mean and dynamic wall-shear stress measurements will be presented and finally, some conclusions will be drawn.

2. Description of the micro-pillar sensor MPS^3

The micro-pillar sensor principle is based on thin cylindrical structures which bend due to the fluid forces, and as such the technique belongs to the indirect group of sensors

since the wall-shear stress is derived from the relation between the detected velocity gradient in the viscous sublayer and the local surface friction. Several other methods such as wall-wire measurements and different micro-cantilevers have been proposed to indirectly measure the wall-shear stress by applying its relation to the near-wall velocity gradient in the viscous sublayer in turbulent flows. Durst et al. (1996) and Kähler et al. (2006) propose to determine the local wall-shear stress by evaluation of the near-wall velocity gradient using LDA (laser-doppler anemometry) or micro-PIV.

The pillars are manufactured from the elastomer polydimethylsiloxane (PDMS, Dow Corning Sylgard 184) at diameters in the range of microns such that they are flexible and easily deflected by the fluid forces to ensure a high sensitivity of the sensor. A single pillar is shown in Fig. 1 and a complete micro-pillar array as it is used to assess the spatial wall-shear stress distribution is illustrated in Fig. 1.

Mechanical models (Fig. 1) of the micro-pillar for static and dynamic loads have been discussed in Große and Schröder (2008). However, these models can only serve as estimates of the pillar response to shear load, since an inevitable uncertainty in the exact definition of the pillar geometry and the material properties due to the remaining variance in the manufacturing conditions, i.e., in determining the second moment of inertia I and Young's modulus E of the poly-dimethylsiloxane (PDMS) silicone, prevents to exactly determine the quantitative pillar bending. Especially in the case of the dynamic response function, effects from internal viscous material damping can be only roughly determined and the influence of the pillar non-linearity close to the pillar base on the dynamic response function cannot be easily approximated.

Since the analytical models serve only as a qualitative estimate of the static and dynamic pillar response, static and dynamic calibrations are necessary prerequisites. A static calibration performed in linear shear flow evidences good qualitative agreement with the predicted pillar deflection.

Note that the small detectable forces of the fluctuating wall-shear stress require a small stiffness of the sensor which consequently results in a lower natural frequency and dynamic bandwidth of the sensor structure. However, to measure the mean and fluctuating components of the wall-shear stress in a turbulent flow, a large dynamic bandwidth is necessary.

The highest characteristic frequencies are related to the smallest scale structures in turbulent flows. These smallest scales are defined by the Kolmogorov length scale l_k (Hinze, 1959; Tennekes and Lumley, 1999). In turbulent pipe flows, the ratio between the Kolmogorov length scale l_k and integral scale l_t can be expressed by $l_k/l_t \sim Re_t^{-3/4}$, where $Re_t = (\overline{u'^2})^{1/2} l_t/\nu$ is the Reynolds number based on the integral scale l_t and the characteristic velocity of the large-scale eddies represented by the integral scale l_t. The integral scale l_t can be assumed to be approximately $0.1\,R$ (Rotta, 1972), where $R = 0.5\,D$ is the radius of the pipe. The eddy velocity can be approximated by the intensity of the velocity fluctuations and is as such $(\overline{u'^2})^{1/2} \approx 0.1 U_b$, where U_b is the bulk velocity (Tennekes and Lumley, 1999). The ratio of the convective time scale $(U_b/R)^{-1}$ and the Kolmogorov time scale T_k can be expressed as $T_k(U_b/R) \approx T_k(\overline{u'^2})^{1/2}/l_t \sim Re_t^{-1/2}$. This yields the highest frequencies to be approximately 250 Hz at the highest Reynolds number based on the bulk velocity $Re_b \approx 20,000$. The corresponding lengths scales of the smallest structures range in the order of 60–70 μm. Numerical simulations by Moser et al. (1999) and del Álamo et al. (2004) also indicate the highest frequencies of the velocity fluctuations in the streamwise direction of turbulent channel flow at comparable Reynolds numbers and wall distances of approximately $y^+ = 5$, i.e., at the upper limit of the viscous sublayer, to be approximately 250 Hz.

As such, it is necessary that the sensor captures this frequency spectrum best with a constant transfer function and with a negligible phase lag. This requires a high enough eigenfrequency of the sensor structure. An analytical estimate and the experimental determination of the resonance frequency of the sensor used in the present study show the undamped eigenfrequency of the structure to be at approximately 2000 Hz. The damped eigenfrequency in water as surrounding medium was determined to be in the order of 1100 Hz, i.e., the dynamic bandwidth can be considered high

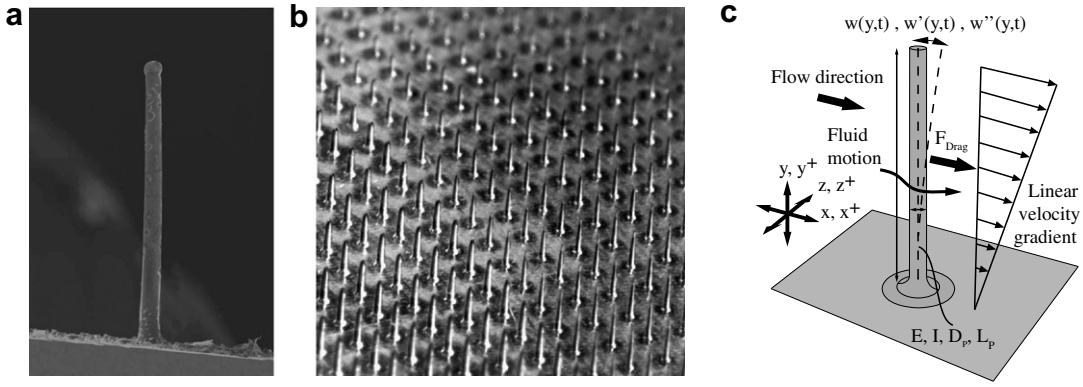

Fig. 1. (a) Scanning electron microscope image of a single pillar and (b) image of a pillar array. (c) Mechanical model of the pillar sensor.

enough to detect the frequency spectrum of the fluctuating wall-shear stress at the Reynolds numbers in the experiments. For further details, see Große and Schröder, 2008.

To enable a sufficiently high sensitivity the sensor possesses an optimum height under the restriction of the validity of the linear relation between the wall-shear stress and the near-wall velocity gradient. That is, the sensor needs to be fully immersed in the flow field for which the linear velocity gradient is guaranteed. Hence, the height of the viscous sublayer limits the height of the pillars. For most turbulent flows of low to moderate Reynolds numbers the height of the viscous sublayer is in the order of 80–1000 μm. These sensor heights L_p have already successfully been manufactured. Furthermore, the current manufacturing process allows a wide range of possible geometric properties of the sensors leading to aspect ratios L_p/D_p between the pillar length L_p and the mean diameter D_p of up to 15–25.

The low intrusiveness of the sensor due to the symmetric and smooth curvature has been examined using micro-PIV (micro particle-image velocimetry) and streakline visualizations of the local flow field around the pillar structure (Große et al., 2006). The results showed the flow past the pillar to be well in the Stokes regime for the typical range of Reynolds numbers $Re_{D_p}(y) = U(y)D_p/\nu$ based on the pillar diameter D_p and the mean velocities in the viscous sublayer $U(y)$ of the turbulent flows of interest.

The sensor concept allows the two-dimensional detection of the fluid forces, since the symmetric geometry has no preferred sensitivity direction. That is, the micro-pillar sensor enables to measure the two wall-parallel components of the drag force. The optical detection principle leads to an extremely high local resolution of the planar wall-shear distribution.

While most thermal or MEMS sensors based on piezoresistive or strain gages devices require secondary structure or data read-out devices at the sensor base thereby impeding the maximum number of sensors or the minimum lateral spacing of single sensors in arrays, the micro-pillar sensor needs no such additional devices and there exist no additional constraints concerning the spatial resolution of the sensor. The impeding limitation is rather the local disturbance of the flow field by the pillar structure and the interference of neighboring pillars. However, due to the Stokes flow, there is only a local impact on the flow field in a region of two to four diameters downstream of the sensor (Große et al., 2006) such that an extremely high spatial resolution can be achieved. The lateral spacing has been chosen approximately equal to the pillar length L_p, i.e., 15–25 D, and as such, a spatial resolution of the wall-shear stress distribution in the order of 4–5 viscous units can be achieved. This allows sensor arrays with spatial resolutions comparable to the characteristic turbulent flow length scale. However, it goes without saying that the maximum number of sensors, which can be evaluated simultaneously with a single camera is limited by the need for a high enough optical resolution. As such, the chosen optical magnification, the pillar geometry – influencing the sensitivity of the structure – and the field of view have to be chosen carefully and with respect to each other and needless to say in compliance with the flow field restrictions.

The sensor structure has a minimum dimension in the wall-parallel plane thereby reducing the spatial averaging. For typical Reynolds numbers the wall-parallel dimension of the sensor in viscous units is $D_p^+ \leqslant 1$, where $D_p^+ = u_\tau D_p/\nu$. However, the micro-pillar sensor causes a spatial averaging of the velocity field along the cylinder axis. The effect will be discussed in Section 4.

From the above discussion it can be concluded, that finding an optimum geometry of the pillar is a difficult task, and the decision needs to be taken with great care since the aforementioned fluid mechanical restrictions and sensor sensitivity based requirements as well as further structure mechanical considerations need to be addressed.

3. Experimental setup

The flow facility, the micro-pillar setup, the optical detection principle and the achievable accuracy are explained in more detail in Große and Schröder (2008) and only a brief overview will be given here.

3.1. Flow facility

The experiments were performed in a pipe facility at the Institute of Aerodynamics. The pipe possesses a diameter of $D = 40$ mm. The fluid used in the measurements is deionised water at a temperature $T = 20$ °C. During the measurements the temperature varies less than 0.1 °C. The Reynolds number based on the bulk velocity $Re_b = U_b D/\nu$ is determined from the measured volume flux V. Measurements of the wall-shear stress have been performed at Reynolds numbers $Re_b = 10,000$–$20,000$, which corresponds to Reynolds numbers $Re_\tau = 630$–1150, where Re_τ is based on the friction velocity u_τ and the pipe diameter D.

The fluid enters through a flow straightener with 5 mm core size followed by a 0.2 mm fine mesh. A tripping device consisting of a circular ring generating a contraction ratio of 0.85 is installed 40 D upstream of the measurement position. The fluid exits the measurement section into an open reservoir and flows through a heat exchanger to maintain a constant fluid temperature.

Particle-image velocimetry (PIV) measurements at Reynolds numbers Re_b ranging from 5000–20,000 confirm the character of the fully developed turbulent pipe flow in the measurement section to be consistent with experimental and numerical results from the literature.

For turbulent pipe flow values of the mean wall-shear stress are well known, such that a comparison of the experimental results with the data from the literature will allow to evaluate the capability of the sensor MPS^3 to determine the mean turbulent wall-shear stress. Generally, the wall-shear stress can be expressed by

$$\tau = \lambda \rho U_b^2/8, \tag{1}$$

where λ is the friction factor. For turbulent flow in a smooth circular pipe, Prandtl and von Kármán (Schlichting, 1958) provide a formula for the friction factor λ

$$\frac{1}{\sqrt{\lambda}} = 2.0 \cdot \log_{10}\left(Re_b\sqrt{\lambda}\right) - 0.8. \quad (2)$$

This allows to easily determine the theoretical wall-shear stress for turbulent pipe flow and also the Reynolds number based on the friction velocity Re_τ.

3.2. Micro-pillar sensor setup

The micro-pillar sensor used for measurements of the wall-shear stress is mounted in a 1 mm cannula, which can be placed very exactly through a hole in the pipe wall. Note, the maximum local disturbance due to the flat surface of the sensor mount and the curvature of the pipe is $\approx 3 \cdot 10^{-4}\ D$ which corresponds to $0.35y^+$ at the highest Reynolds numbers in the experiments, i.e., additional disturbances can be neglected.

The micro-pillars have a height L_p of 350 μm and a mean diameter D_p of approximately 45 μm. The height corresponds to about 3–10 viscous units for the Reynolds numbers in the experiments. At the highest Reynolds numbers the sensor slightly exceeds the thickness of the viscous sublayer.

The sensor displacement from a reference position at no velocity is observed using a highly magnifying macro lens mounted on a Fastcam 1024 PCI high-speed camera. The camera is operated at 125 Hz and 2000 Hz. Images (51,200) are recorded for each measurement at both recording frequencies resulting in a total period of 7 min and 26 s, respectively. During this timespan a particle with bulk velocity U_b travels a distance of 2600–5200 D at 125 Hz and 160–320 D at 2000 Hz depending on the Reynolds number.

The error to determine the pillar-tip displacement is less than 2.5% and 0.5%, at the lowest and highest Reynolds numbers in the experiments, respectively. Using the relation between pillar deflection and shear stress determined from the static calibration the smallest detectable wall-shear stress becomes approximately 10 mPa with the current setup. Note, the optical detection principle and the achievable accuracy are discussed in depth in Große and Schröder (2008).

4. Results

Before the actual results from the dynamic wall-shear stress measurements in turbulent pipe flow will be discussed we would like to shortly address the problem of the comparability of results obtained with the present technique with wall-shear stress data available in the literature.

Although there exists an increasing number of MEMS sensor devices with a measurement principle similar to the one of the presented sensor, there is almost no comparable wall-shear stress data available in the literature that would allow a direct quantitative comparison of the results to the ones discussed in the present manuscript.

Even with data of the instantaneous velocity profile in the viscous sublayer, e.g. from DNS data, it would still be an extremely difficult task to compare the results measured with the sensor to such data since further assumptions would need to be made to calculate a theoretical deflection of the pillar from the given velocity fields.

Consequently, to judge the quality of the micro-pillar sensor to correctly detect the dynamic wall-shear stress, the sensor was applied under well-known flow conditions to check the results against the data available in the literature. As such we compare the results of the present study to the existing results thereby acknowledging that the data has been obtained in different ways.

In this context, the comparability of integral and pointwise data acquisition should briefly be discussed. An estimation of the wall-shear stress by integration of the flow field in the vicinity of the wall is only valid under the assumption of a linear velocity gradient in the viscous sublayer. The measurement of the wall-shear stress using hot-wires installed at a distinct height in the viscous sublayer is based on the same assumption. However, in the case of hot-wires only the velocity at a distinct wall distance is used to calculate the local wall-shear stress.

Unfortunately, it is difficult to evidence how far the instantaneous wall-shear stress correlates with the instantaneous velocity at a distinct point or the velocity distribution in the viscous sublayer. On what concerns mean and lower-order moments of the fluctuations, i.e., the fluctuation intensity, Alfredsson et al. (1988) and others showed the mean velocity gradient to be linear and furthermore, the mean fluctuation intensity to also possess a rather constant value within the viscous sublayer. However, there exists a controversial discussion on the latter subject and this point will further be discussed in Section 4.2. Furthermore, the correlation between $u(y)$ and $\partial u/\partial y|_{wall}$ is very high up to $y^+ = 5$ (Eckelmann, 1974) thereby indicating a high level of similarity of the momentary velocity in the viscous sublayer and the local wall-shear stress, i.e., the velocity profile and the velocity at a distinct point in the vicinity of the wall can be assumed to serve as good representatives of the local wall-shear stress and its lower-order moments.

4.1. Mean wall-shear stress

In Fig. 2 the results from the present experimental study are juxtaposed to values calculated by Eqs. (1) and (2) for the friction factor for turbulent flow in hydraulically smooth pipes. The results show excellent agreement with the analytical distribution and evidence the sensor to be capable of correctly detecting the mean wall-shear stress in turbulent flows.

At low Reynolds numbers in the experiments, i.e., at $Re_b \leqslant 12,000$, the data scatter around the theoretical value of the mean wall-shear stress. This can also be observed in Fig. 2, where the measured friction velocity u_τ is compared

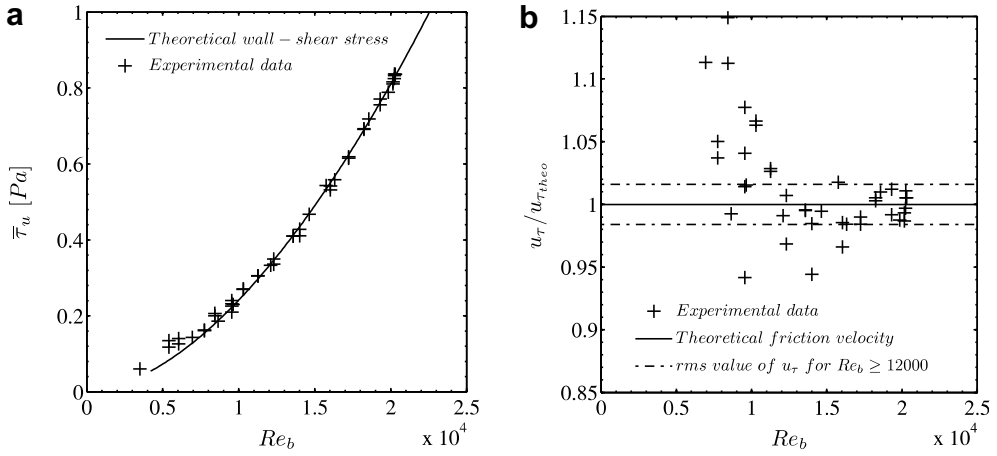

Fig. 2. (a) Mean streamwise wall-shear stress $\overline{\tau}_u$ at turbulent pipe flow compared to the solution calculated by formulas 1 and 2. (b) Ratio of the friction velocity u_τ compared with the theoretical friction velocity $u_{\tau_{\text{theo}}}$. The dash-dotted lines indicate the rms value of the measured wall-shear stress at $Re_b \geqslant 12,000$.

with theoretical values calculated by Eq. (2). The stronger error in the estimate of the wall-shear stress is due to the very low values of the mean wall-shear stress of ≈ 0.1 Pa and the chosen optical resolution during the measurements leading to a pillar-tip deflection in the order of 1 *px* and hence, to an increased error in the estimate of the wall-shear stress.

The use of higher magnifying optics especially at low Reynolds numbers would increase the optical resolution and hence, would allow a higher accuracy of the system. Furthermore, the use of more slender pillars with higher deflections would enhance the sensitivity of the wall-shear stress sensor principle. Measurements with an adapted setup and more sensible pillars will be performed in the future to show the applicability of the sensor even at lower Reynolds numbers.

The results at $Re_b \geqslant 12,000$ scatter only slightly around the theoretical value of the mean friction velocity $u_{\tau_{\text{theo}}}$. Using the current experimental conditions an rms value of approximately $0.0175 u_{\tau_{\text{theo}}}$ is achieved. The rms value calculated from the results at $Re_b \geqslant 12,000$ is also plotted in Fig. 2.

Although the sensor at a height of $L_p = 350$ μm partly exceeds the linear velocity region at the highest Reynolds numbers, the detected wall-shear stress follows the predicted trend. This is most likely due to the lowered pillar structure at higher shear rates. Furthermore, it needs to be taken into account that only the upper part of the pillar extends into a region, where the linear velocity gradient is no longer valid. Due to the integration of the velocity field along the sensor the beginning non-linearity of the velocity field at $y^+ \geqslant 7$ influences the pillar reaction only slightly.

4.2. Wall-shear stress intensity, skewness, and flatness

While the linear behavior of the mean velocity gradient in the viscous sublayer is commonly accepted, there are controversial results and opinions on the fluctuation intensity $u'/\overline{U}$ in the literature, where $\overline{U}$ is the mean streamwise velocity. Often a value of $\tau'_u/\overline{\tau}_u = 0.4$, where $\overline{\tau}_u$ is the mean wall-shear stress and a value of $u'/\overline{U} = 0.4$ in the near vicinity of the wall is assumed, where 'near vicinity' is understood as in the order of one Kolmogorov length. Note, the wall-shear stress and velocity fluctuations, $\tau'_u/\overline{\tau}_u$ and $u'/\overline{U}$, respectively, are directly related to each other in the vicinity of the wall and as such can be directly compared.

The distribution of the fluctuations in the viscous sublayer is of major importance for indirect measurement techniques. For channel flow, Kreplin and Eckelmann (1979) report a value of $u'/\overline{U} = 0.25$ at the wall with a plateau at $y^+ = 3$–6 and values of $u'/\overline{U} = 0.36$–0.37 before the fluctuation intensity decays. Wietrzak and Lueptow (1994) compile several results from experimental studies and DNS findings for channel and boundary layer flow with values of $\tau'_u/\overline{\tau}_u$ ranging from 0.1 to 0.4. Alfredsson et al. (1988) found the values of $u'/\overline{U}$ to be at a constant level of 0.4 up to values of $y^+ = 4$ in turbulent channel flow. This trend is also supported by the results obtained by Khoo et al. (1997). For higher values of y^+, the authors report the rms value to decrease to 0.33–.3. Numerical calculations for channel flow performed by Moser et al. (1999) at Reynolds numbers ranging from $Re_H = 5600$–$21,000$, where $Re_H = U_b H/\nu$ is the Reynolds number based on the bulk velocity U_b and the channel height H, showed the values to be $\tau'_u/\overline{\tau}_u = 0.38$–$0.4$.

Fig. 3 shows the measured rms values $\tau'_u/\overline{\tau}_u$ to be approximately 0.39 for the streamwise component at the lowest Reynolds number in the experiments and to decrease with the Reynolds number to values of $\tau'_u/\overline{\tau}_u = 0.33$–$0.34$ in the range of $Re_b = 10,000$–$20,000$. The micro-pillar sensor protrudes further into the near-wall region at higher Reynolds numbers and this causes a spatial averaging up to higher values of y^+, i.e., the observed decrease in the present study is in good agreement with the findings of Khoo et al. (1997) and Alfredsson et al.

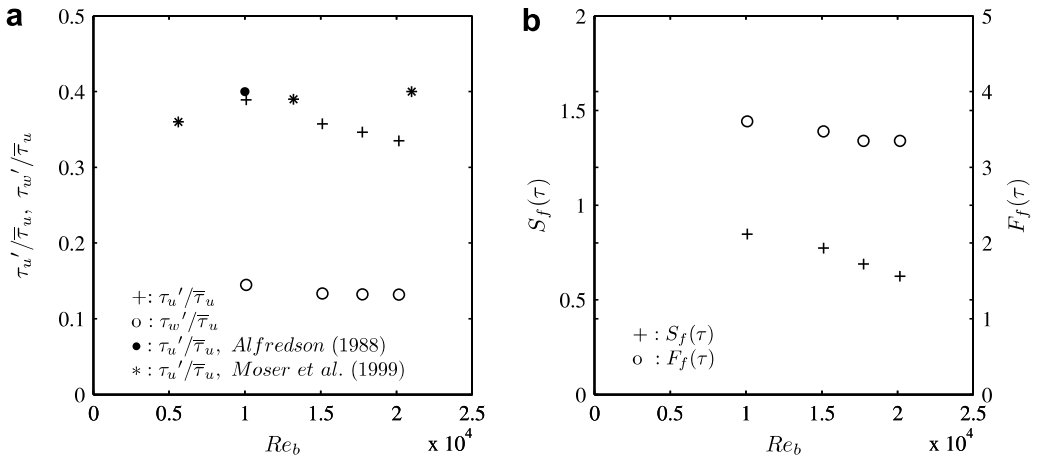

Fig. 3. (a) RMS values of the streamwise $\tau_u'/\overline{\tau}_u$ and spanwise wall-shear stress fluctuations $\tau_w'/\overline{\tau}_u$. (b) Skewness $S_f(\tau)$ and flatness $F_f(\tau)$ of the streamwise wall-shear stress fluctuations τ_u.

(1988). Consequently, it has to be taken into account that the sensor integrates the flow field along the wall-normal direction and hence, a gradient of any flow property along the sensor length can hardly be detected. Therefore, at the present state, it cannot be determined from the results obtained with the actual setup whether or not the intensity of the wall-shear stress fluctuations $\tau_u'/\overline{\tau}_u$ is constant within the viscous sublayer. It can only be stated that the mean value of $\tau_u'/\overline{\tau}_u$ in the vicinity of the wall is represented by the values noted above.

The measured spanwise component $\tau_w'/\overline{\tau}_u$ in Fig. 3 is about 0.15 at the lowest Reynolds number in the experiments. At higher Reynolds numbers the intensity decreases to values of $\tau_w'/\overline{\tau}_u \approx 0.13$. This is in good agreement with the findings of Kreplin and Eckelmann (1979). Their results show the spanwise component to reach a maximum intensity of $\tau_w'/\overline{\tau}_u = 0.2$ at wall distances $y^+ = 3$–4 followed by a strong decay to values of approximately 0.1. Note, the pillar sensor tends to average the slope of the fluctuation intensity $\tau_w'/\overline{\tau}_u$ and to underestimate the value in the vicinity of the wall. Using smaller pillars with $L_p = 3$–4 y^+ would reduce this effect.

The skewness of the fluctuations in Fig. 3 is $S_f(\tau) = 0.85$ at the lower Reynolds numbers and decreases slightly to $S_f(\tau) = 0.6$ at higher Reynolds numbers. Values of $S_f(u) \approx 1.0$ are reported in Alfredsson et al. (1988) and in Khoo et al. (1997) for hot-wires located at $y^+ \leqslant 4$ whereas Fernholz and Finley (1996) report a $S_f(u)$ of 1.2–1.3 in the near-wall region and a vanishing $S_f(u)$ at values of $y^+ \geqslant 12$.

The findings for the flatness $F_f(\tau)$ in Fig. 3 show a similar behavior. It reaches $F_f(\tau) = 3.7$ at lower Reynolds numbers and decreases to a value of 3.3 at higher Reynolds numbers. Similarly high values are reported in Fernholz and Finley (1996) at $y^+ \leqslant 4$.

Note, the flatness and skewness of the velocity fluctuations are reported to decay strongly with increasing y^+. As such, it has to be taken into account that the proposed sensor integrates the flow field along the wall-normal direction. Hence, any non-constant distribution of statistical turbulence characteristics along the sensor length can hardly be detected and consequently, values of such terms measured with the micro-pillar sensor can not be treated as a suitable direct representative of the corresponding wall-shear stress characteristics. Especially higher-order moments of the velocity fluctuations in the vicinity of the wall such as the skewness and the flatness show a non-constant distribution, which is why these wall-shear stress properties can not be determined by integrating the corresponding velocity fluctuation quantities. The detected decreasing skewness and flatness evidenced in Fig. 3 at higher Reynolds numbers result from the aforementioned inadequate sensor length and an integration of fluctuations along the wall-normal direction up to higher values of y^+. An even stronger, but similar trend has already been observed in earlier measurements with higher pillars.

4.3. Frequency spectra

The frequency spectra of the streamwise wall-shear stress fluctuations τ_u are plotted in Fig. 4. Spectral densities $\Phi^+(f^+)$ have been calculated using formula given in Press et al. (2007). For each recording frequency the power spectra have been normalized such that $\int_0^\infty \Phi^+(f^+)\mathrm{d}f^+ = \tau_u'$. The spectral densities $\Phi^+(f^+)$ and frequencies f^+ are scaled with inner and outer variables as well as with a combination of both, i.e., a mixed scaling is applied.

It can be concluded from the results that mixed scaling provides the best collapse of the complete frequency spectra. The high-frequency parts of the fluctuations collapse best for inner and reasonably for mixed scaling, whereas outer scaling leads to diverging spectral densities at high frequencies. The low-frequency parts of the fluctuations collapse best for mixed scaling, whereas inner scaling causes a strong spread of the spectral density distributions at low frequencies. This result is also reported by

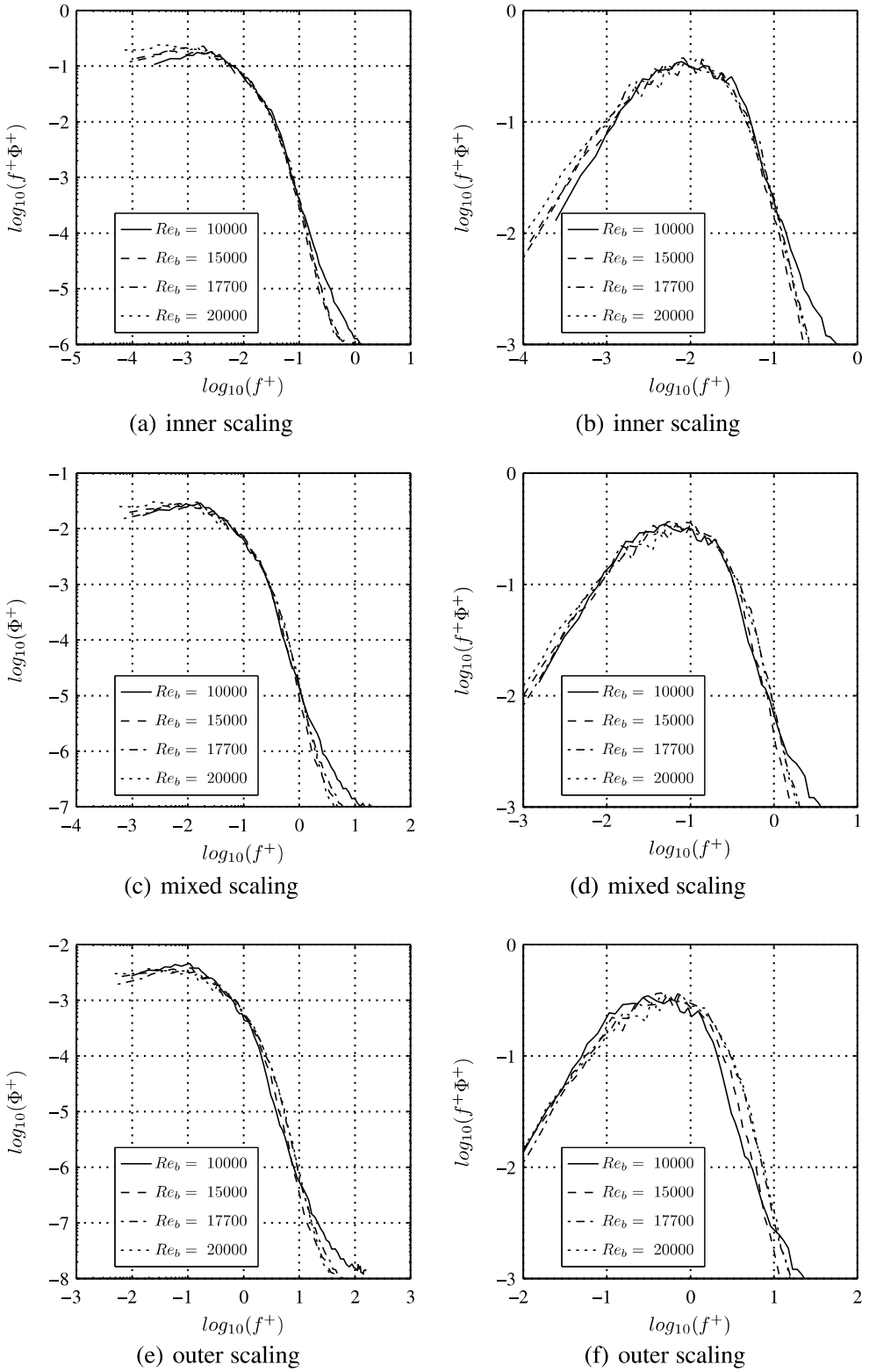

Fig. 4. Power spectra Φ^+ (left) and pre-multiplied power spectra $f^+\Phi^+$ (right) of τ_u as functions of the frequency f^+ in inner, mixed, and outer scaling at different Reynolds numbers.

Alfredsson and Johansson (1984) and Jeon et al. (1999) for spectral densities obtained experimentally and by DNS of turbulent channel flow.

The question whether or not wall-shear stress or velocity fluctuations in the near-wall region of turbulent boundary layers, i.e., the buffer layer or low logarithmic region, scale

with inner or outer variables has very controversially been discussed.

Most authors applied inner scaling to their results from the buffer region but it seems that mixed scaling would have rather led to the Reynolds number independence of the data. Madavan et al. (1985) show results from skin-friction measurements in turbulent boundary layer flow at different Reynolds numbers and assume wall-shear stress spectra to scale with inner variables. The spectral data presented contains only the low-frequency end of the complete frequency spectrum such that it is hard to know whether or not the applied scaling also holds for the high-frequency content of the turbulent fluctuations. Alfredsson and Johansson (1984) report velocity fluctuations in the buffer layer of turbulent channel flow at Reynolds numbers Re_b between 13,800 and 123,000 to collapse best when mixed scaling is applied. The experimental results from Sreenivasan and Antonia (1977) and Madavan et al. (1985) were juxtaposed by Jeon et al. (1999) and evidence no reasonable collapse of the spectral densities in a Reynolds number range $Re_\tau = 289$–3060 when inner or outer scaling is applied. As mentioned before this contradicts with the inner scaling that Madavan et al. (1985) applied to their own data.

In conclusion, it can be suggested from the present results that the use of mixed scaling variables, which seems most reasonable for velocity fluctuations in the buffer and log region in wall-bounded flows, also applies for the wall-shear stress fluctuations over the investigated Reynolds number range for turbulent pipe flow.

Nonetheless, it has to be kept in mind that the scaling of power spectra is very sensitive to the determination of the correct friction velocity. Furthermore, the experimental determination suffers strongly from spatial averaging caused by an inappropriate dimension of the detection devices, i.e., especially small scale structures are affected by the integration of the turbulent signal along the sensor dimensions.

Pre-multiplied power spectra showing $f^+\Phi^+$ versus f^+ are also given in Fig. 4. This illustration allows to easily recognize the frequency range of the energy containing vortices. The results show a maximum in the spectral power $f^+\Phi^+$ for inner scaling at $fv/u_\tau^2 \approx 10^{-2}$ and for outer scaling at $f\delta/U_0 \approx 4$–5×10^{-1}.

A comparison of the results to power spectral densities reported by del Álamo et al. (2004) at turbulent channel flow at Reynolds numbers based on the friction velocity and the channel half-height $Re_{\tau,\mathrm{Ch}} = u_\tau h/v = 180,\ 550,$ and 950 is given in Fig. 5. Note, at turbulent pipe flow, the pipe diameter is used to define the Reynolds number Re_τ. That is, to compare the channel and the pipe data the Re_τ values of the channel flow need to be doubled, i.e., $\hat{Re}_\tau = 2Re_{\tau,\mathrm{Ch}} = 360$, 1100, and 1900. The data can be found on the web at http://torroja.dmt.upm.es/ or http://turbulence.ices.utexas.edu/. Since no DNS data of the wall-shear stress is available the velocity fluctuation spectra at the lowest available position to the wall have been used. At the investigated Reynolds numbers, this lowest position is in the range of $y^+ = 4.7$–5.4.

A direct comparison of the spectra is not possible since the DNS based data are computed as a function of wavenumber k, whereas those from the experiments are calculated from time series and as such are a function of frequency f. The two spectra can be related to each other through the Taylor hypothesis, i.e., $2\pi f = kU_c$. Herein, the quantity U_c is the mean convection velocity of the velocity fluctuations. Following Kim and Hussain (1993), the convection velocity of the streamwise velocity fluctuations at $y^+ \leqslant 5$ is approximately $U_c = 10\ u_\tau$ such that $2\pi f = 10\ ku_\tau$.

In Fig. 5 the spectra $\widetilde{\Phi}$ and pre-multiplied spectra $\tilde{f}\widetilde{\Phi}$ from the DNS and the measurements are juxtaposed. The

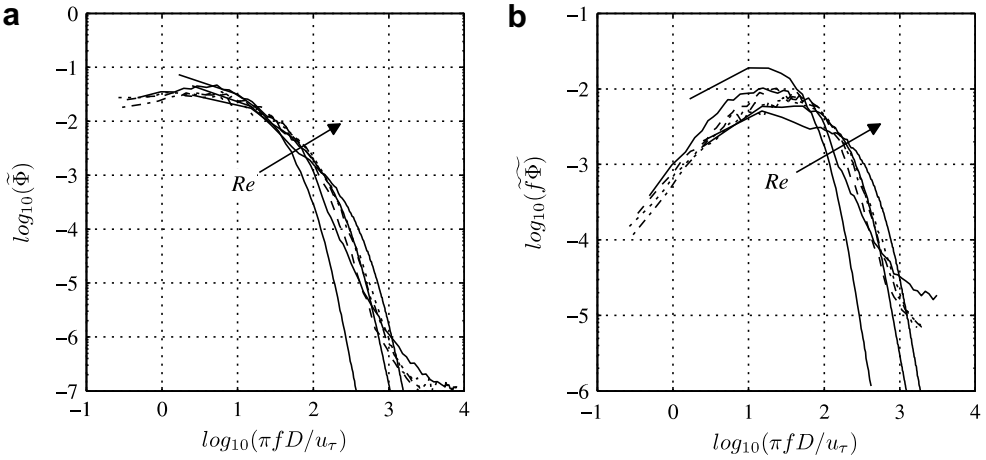

Fig. 5. (a) Power spectra $\widetilde{\Phi}$ and (b) pre-multiplied power spectra $\tilde{f}\widetilde{\Phi}$ of wall-shear stress fluctuations τ_u as functions of the normalized frequency $\tilde{f} = \pi fD/u_\tau$ of experiments at $Re_b = 10,000$–$20,000$ corresponding to $Re_\tau = 630$–1150 compared to spectra of velocity fluctuations u at $y^+ \approx 5$ from turbulent channel DNS at $\hat{Re}_\tau = 360$, 1100, and 1900 (del Álamo et al., 2004). For symbols of the experimental data see Fig. 4, thick continuous lines: DNS data.

DNS spectrum at $\hat{Re}_\tau = 1100$ shows excellent agreement with the findings in the present study at $Re_b = 20,000$, which corresponds to $Re_\tau = 1150$. This good qualitative and quantitative correspondence in the spectral distributions evidence the ability of the sensor structure to also detect the higher frequency content of the wall-shear stress. The drift of the experimental results from the DNS data at the highest frequencies is defined by the minimum experimental resolution.

5. Conclusion

The wall-shear stress sensor concept MPS^3 to measure the two-dimensional wall-shear stress distribution in turbulent flow has been introduced. The sensor is based on flexible micro-pillars protruding into the near-wall region of turbulent flow.

To judge the quality of the micro-pillar shear stress sensor MPS^3 to correctly detect the wall-shear stress, skin-friction measurements in a well-defined turbulent pipe flow at Re_b ranging from 10,000 to 20,000 have been performed. The results are in convincing agreement with data available from the literature and evidence the micro-pillar shear stress sensor to correctly detect the mean wall-shear stress with an error of approximately $0.0175u_{\tau_{theo}}$ at Re_b ranging from 12,000 to 20,000.

Characteristics of the dynamic wall-shear stress such as the fluctuation intensity were shown to be in the order of values reported in the literature. From these results it can be concluded that the measurement of mean and fluctuating wall-shear stress by determining the velocity gradient in the vicinity of the wall is generally possible. Nonetheless, it has to be taken into account that the proposed sensor integrates the flow field along the wall-normal direction. Hence, any non-constant distribution of statistical turbulence characteristics along the sensor length can hardly be detected and consequently, values of such terms measured with the micro-pillar sensor can not be treated as a suitable direct representative of the corresponding wall-shear stress characteristics. Especially higher-order moments of the velocity fluctuations in the vicinity of the wall such as the skewness and the flatness show a non-constant distribution, which is why these wall-shear stress properties can not be determined by integrating the corresponding velocity fluctuation quantities. The experimentally determined spectral densities of the wall-shear stress fluctuations show good agreement with DNS data from the literature at comparable Reynolds numbers.

A great advantage of the micro-pillar concept is the possibility to detect the planar wall-shear stress distribution by using arrays of micro-pillars at high spatial resolution. To be more precise, the pillar technique allows the simultaneous detection of the two-dimensional distribution of streamwise and spanwise wall-shear stress at up to 1000 points with a spatial resolution of approximately 5 viscous units.

The sensor concept is reasonably robust and can be easily mounted on almost any surface. The presented sensor structure needs no additional infrastructure on the wall thereby reducing additional flow disturbances. Only customary high-speed optics is needed to detect the sensor array. This makes the novel technology a simple technique to visualize and measure the planar turbulent wall-shear stress distribution of the two wall-shear stress components. The question whether or not the technique can also be considered 'low-cost' is up to the reader. Quite recently, a brand-new high-speed camera system has been introduced that enables recordings at frame rates of up to 5 kHz at resolutions of 1 *Megapixel*. It is needless to say that the costs of this camera still represent some kind of barrier.

Acknowledgement

The authors are grateful for the financial support by the DFG Priority Program 'Nano- and Microfluidics' – SPP 1164.

References

Alfredsson, P.H., Johansson, A.V., 1984. Time scales in turbulent channel flow. Physics of Fluids 27 (8), 1974–1981.

Alfredsson, P.H., Johansson, A.V., Haritonidis, J.H., Eckelmann, H., 1988. The fluctuating wall-shear stress and the velocity field in the viscous sublayer. Physics of Fluids 31 (5), 1026–1033.

Brücker, C., Spatz, J., Schröder, W., 2005. Feasibility study of wall-shear stress imaging using microstructured surfaces with flexible micropillars. Experiments in Fluids 39, 464–474.

Chen, J., Fan, Z., Zou, J., Engel, J., Liu, C., 2003. Two-dimensional micromachined flow sensor array for fluid mechanics studies. Journal of Aerospace Engineering 16 (2), 85–97.

del Álamo, J.C., Jiménez, J., Zandonade, P., Moser, R.D., 2004. Scaling of the energy spectra of turbulent channels. Journal of Fluid Mechanics 500, 135–144.

Dijkstra, M., van Baar, J.J., Wiegerink, R.J., Lammerink, T.S., de Boer, J.H., Krijnen, G.J.M., 2005. Artificial sensory hairs based on the flow sensitive receptor hairs of crickets. Journal of Micromechanics and Microengineering 1, 132–138.

Durst, F., Kikura, H., Lekakis, I., Jovanovic, J., Ye, Q., 1996. Wall-shear stress determination from near-wall mean velocity data in turbulent pipe and channel flows. Experiments in Fluids 20, 417–428.

Eckelmann, H., 1974. The structure of the viscous sublayer and the adjacent wall region in a turbulent channel flow. Journal of Fluid Mechanics 65, 439–459.

Engel, J., Chen, J., Liu, C., Bullen, D., 2006. Polyurethane rubber all-polymer artificial hair cell sensor. Journal of Microelectromechanical Systems 15 (5), 729–736.

Fan, Z., Chen, J., Zou, J., Bullen, D., Liu, C., Delcomyn, F., 2002. Design and fabrication of artificial lateral line flow sensors. Journal of Micromechanics and Microengineering 12, 655–661.

Fernholz, H.H., Finley, P.J., 1996. The incompressible zero-pressure-gradient turbulent boundary layer: an assessment of the data. Progress in Aerospace Sciences 32 (4), 245–311.

Fernholz, H.H., Janke, G., Schrober, M., Wagner, P.M., Warnack, D., 1996. New developments and applications of skin-friction measuring techniques. Measurement Science and Technology 7, 1396–1409.

Große, S., Schröder, W., 2008. Mean wall-shear stress measurements using the micro-pillar shear stress sensor MPS^3. Measurement Science and Technology 19 (1), 015403.

Große, S., Schröder, W., submitted for publication. Two-dimensional wall-shear stress visualization in turbulent duct flows. AIAA Journal.

Große, S., Schröder, W., Brücker, C., 2006. Nano-newton drag sensor based on flexible micro-pillars. Measurement Science and Technology 17, 2689–2697.

Hinze, J.O., 1959. Turbulence, first ed. McGraw-Hill.

Humphrey, J.A.C., Barth, F.G., 2007. Medium flow-sensing hairs: biomechanics and models. In: Casas, J., Simpson, S.J. (Eds.), Insect Mechanics and Control, vol. 34, Advances in Insect Physiology. pp. 1–80.

Jeon, S., Choi, H., Yoo, J.Y., Moin, P., 1999. Space–time characteristics of the wall-shear stress fluctuations in a low-reynolds-number channel flow. Physics of Fluids 11 (10), 3084–3094.

Kähler, C.J., Scholz, U., Ortmanns, J., 2006. Wall-shear stress and near-wall turbulence measurements up to single pixel resolution by means of long-distance micro-PIV. Experiments in Fluids 41 (2), 327–341.

Khoo, B.C., Chew, Y.T., Li, G.L., 1997. Effects of imperfect spatial resolution on turbulence measurements in the very near-wall viscous sublayer region. Experiments in Fluids 22, 327–335.

Kim, J., Hussain, F., 1993. Propagation velocity of perturbations in turbulent channel flow. Physics of Fluids 5 (3), 695–706.

Kimura, M., Tung, S., Lew, J., Ho, C.-M., Jiang, F., Tai, Y.-C., 1999. Measurements of wall-shear stress of a turbulent boundary layer using a micro-shear stress imaging chip. Fluid Dynamics Research 24 (6), 329–342.

Kreplin, H.-P., Eckelmann, H., 1979. Behavior of the three fluctuation velocity components in the wall region of a turbulent channel flow. Physics of Fluids 22 (7), 1233–1239.

Krijnen, G.J.M., Dijkstra, M., van Baar, J.J., Shankar, S.S., Kuipers, W.J., de Boer, R.J.H., Altpeter, D., Lammerink, T.S.J., Wiegerink, R., 2006. MEMS based hair flow-sensors as model systems for acoustic perception studies. Nanotechnology 17, S84–S89.

Lin, Q., Jiang, F., Wang, X.-Q., Xu, Y., Han, Z., Tai, Y.-C., Lew, J., Ho, C.-M., 2004. Experiments and simulations of MEMS thermal sensors for wall-shear stress measurements in aerodynamic control applications. Journal of Micromechanics and Microengineering 14 (12), 1640–1649.

Löfdahl, L., Gad-el-Hak, M., 1999. MEMS-based pressure and shear stress sensors for turbulent flows. Measurement Science and Technology 10, 665–686.

Madavan, N.K., Deutsch, S., Merkle, C.L., 1985. Measurements of local skin friction in a microbubble-modified turbulent boundary layer. Journal of Fluid Mechanics 156, 237–256.

Moser, R.D., Kim, J., Mansour, N.N., 1999. Direct numerical simulation of turbulent channel flow up to $Re_\tau = 590$. Physics of Fluids 11, 943–945.

Naughton, J., Sheplak, M., 2002. Modern developments in shear stress measurement. Progress in Aerospace Sciences 38, 515–570.

Press, W.H., Teukolsky, S.A., Vetterling, W.T., Flannery, B.P., 2007. Numerical Recipes in C. Cambridge University Press.

Rotta, J., 1972. Turbulente Strömungen. B.G. Teubner, Stuttgart.

Schlichting, H., 1958. Grenzschicht-Theorie, third ed. Verlag G. Braun, Karlsruhe.

Sreenivasan, K.R., Antonia, R.A., 1977. Properties of wall-shear stress fluctuations in turbulent duct flow. Journal of Applied Mechanics 44, 389–395.

Tennekes, H., Lumley, J., 1999. A First Course in Turbulence. MIT Press, Cambridge, Massachusetts, and London, England.

Tucker, C., Chen, N., Engel, J., Yang, Y., Pandya, S., Liu, C., 2006. High-sensitivity Bi-directional flow sensor based on biological inspiration of animal haircell sensors. In: Proceedings of the 5th IEEE Sensors Conference 2006.

Wietrzak, A., Lueptow, R.M., 1994. Wall-shear stress and velocity in a turbulent axisymmetric boundary layer. Journal of Fluid Mechanics 259, 191–218.